

# Chapter 4

## Multi-scale modelling of dry granular flows

### 4.1 Introduction

The dynamics of a homogeneous granular flow involve at least three distinct scales: the *microscopic scale*, which is characterised by the contact between grains, the *meso-scale* that represents micro-structural effects such as grain rearrangement, and the *macroscopic scale*, where geometric correlations can be observed (see Figure 4.1). Conventionally, granular flows are modelled as a continuum because they exhibit many collective phenomena. However, on a grain scale, the granular materials exhibit complex solid-like and/or fluid-like behaviour. Recent studies, however, suggest that a continuum law may be unable to capture the effect of inhomogeneities at the grain scale level, such as orientation of force chains, which are micro-structural effects. Discrete element methods (DEM) are capable of simulating these micro-structural effects, however they are computationally expensive. In the present study, a multi-scale approach is adopted, using both DEM and continuum techniques, to better understand the rheology of granular flows and the limitations of continuum models.

### 4.2 Granular column collapse

The collapse of a granular column on a horizontal surface is a simple case of granular flow, however a proper model that describes the flow dynamics is still lacking. Granular flow is modelled as a frictional dissipation process in continuum mechanics but studies showing the lack of influence of inter-particle friction on the energy dissipation and spreading dynamics is surprising. In the present study, the generalised interpolation material point method (GIMPM),

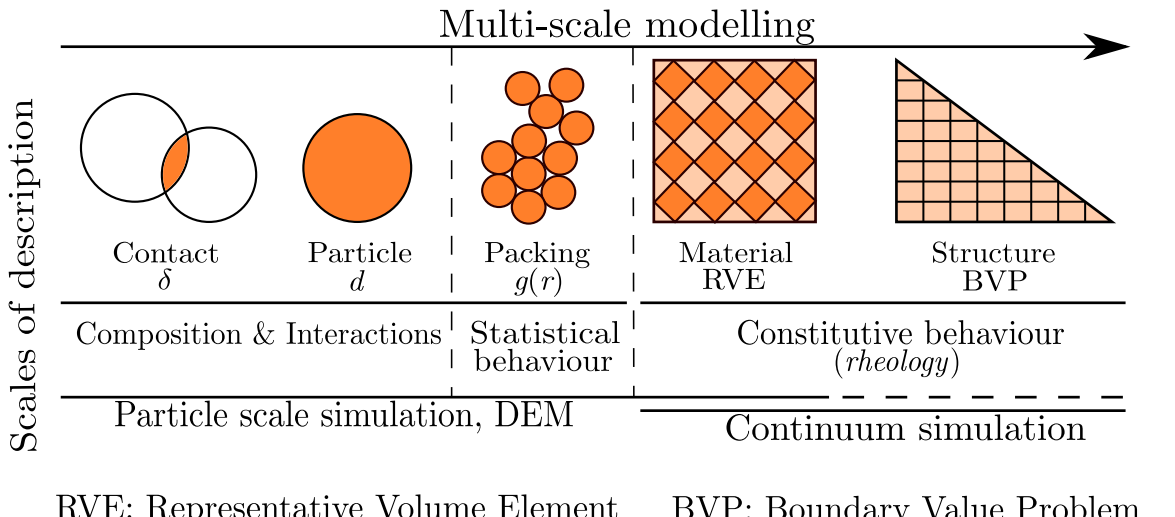


Figure 4.1 Multi-scale modelling of granular materials

- <sup>1</sup> a hybrid Eulerian – Lagrangian approach, is implemented with Mohr-Coloumb failure criterion
- <sup>2</sup> to describe the continuum behaviour of quasi-two dimensional collapse of granular columns.
- <sup>3</sup> The granular column collapse is also simulated using DEM to understand the micro-mechanics
- <sup>4</sup> of the flow.

<sup>5</sup> The granular column collapse experiment involves filling a cylinder of height  $H_0$  and width  $L_0$  with a granular material of mass ‘m’. The granular column is then released *en masse* <sup>6</sup> by quickly removing the cylinder, thus allowing the granular material to collapse onto the <sup>7</sup> horizontal surface, forming a deposit having a final height  $H_f$  and radius  $L_f$ . A computational <sup>8</sup> study on an equivalent two-dimensional configuration (circular disks) was carried out using <sup>9</sup> Discrete Element and Continuum (MPM) approaches.

<sup>10</sup> [Lajeunesse et al. \(2004\)](#) performed axis-symmetric and plane strain tests on granular <sup>11</sup> column collapse. Granular materials when released suddenly on a horizontal surface exhibit <sup>12</sup> transient flow. The mechanism of flow initiation, spreading dynamics and energy dissipation <sup>13</sup> are studied. The experimental configuration used by [Lajeunesse et al. \(2004\)](#) is shown in <sup>14</sup> Figure 4.2. Granular material of mass ‘M’ was poured into a container to form a rectangular <sup>15</sup> heap of length ‘ $L_i$ ’, height ‘ $H_i$ ’ and thickness ‘ $W$ ’. The internal friction angle and the wall <sup>16</sup> friction between the wall and the glass beads measured by [Lajeunesse et al. \(2004\)](#) are listed <sup>17</sup> in Table 4.1. The gate was then quickly removed to release the granular mass that spreads in <sup>18</sup> the horizontal channel until it comes to rest. The final run-out distance ‘ $L_f$ ’ and the collapsed <sup>19</sup> height ‘ $H_f$ ’ were measured. The run-out distance and collapse height were found to exhibit <sup>20</sup> power law relation with the initial aspect ratio ‘ $a$ ’ ( $= H_i/L_i$ ) of the column.

<sup>21</sup> In this study, numerical simulations of the granular column collapse experiments are per-  
formed by varying the initial aspect ratio of the column. Discrete Element Method simulations

## 4.2 Granular column collapse

## 3

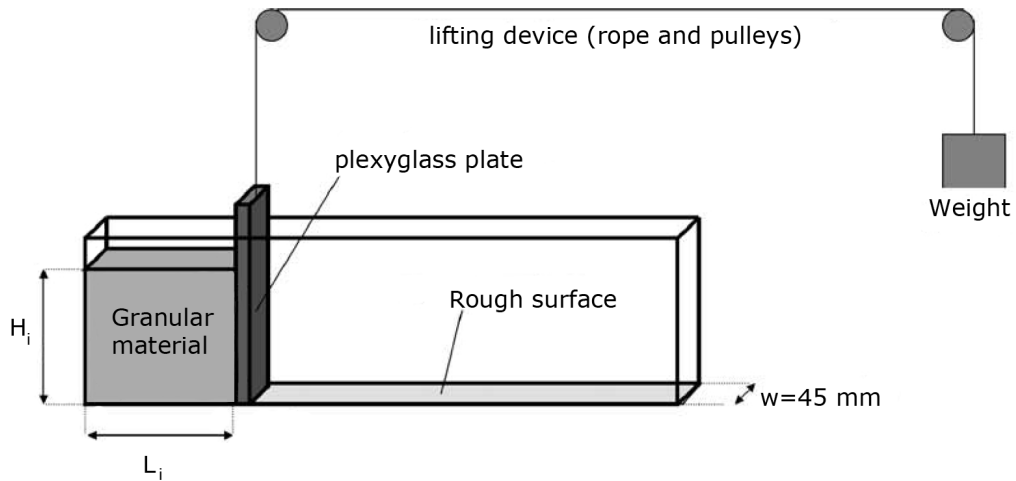


Figure 4.2 Schematic of experimental configuration for 2-D collapse in a rectangular channel, ([Lajeunesse et al., 2004](#))

Table 4.1 Material properties of glass ballotini, ([Lajeunesse et al., 2004](#))

Parameter	Value
Mean diameter	1.15 mm
Repose angle	$22 \pm 0.5^\circ$
Avalanche angle	$27.4 \pm 0.5^\circ$
Wall friction angle	$24.8 \pm 0.2^\circ$

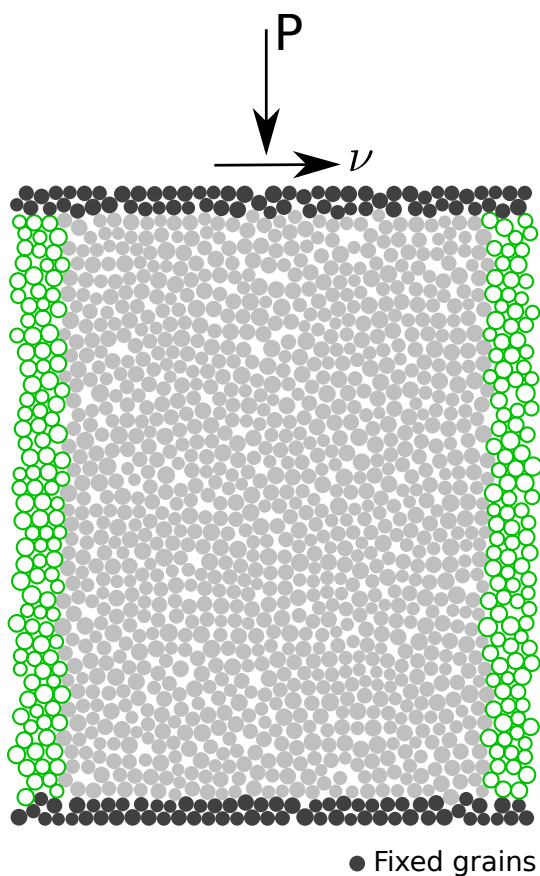


Figure 4.3 Shear test periodic boundary condition

involve modelling the granular column as individual particles. The granular column is prepared by randomly packing poly-disperse grains on a regular lattice and allowing them to undergo free fall due to gravity, forming a randomly packed granular column (see

Krishna Kumar Soundararajan: Add Chapter reference

The grains are allowed to reach a stable equilibrium after undergoing some elastic compressions due to gravity. The overlaps between particles are determined by the stiffness  $k_n$  of the spring in the normal direction. Typically, average overlaps in the range 0.1 to 1.0% are desirable and the spring constant is chosen to produce particle overlaps in this range. The stiffness is determined using the following equation:

$$k_n = \frac{2\pi G}{(1-\nu)[2\ln(\frac{2r}{A})-1]} \quad (4.1) \quad 10$$

$$A = \left[ \frac{2r(1-\nu)f_n}{\pi G} \right]^{\frac{1}{2}} \quad (4.2) \quad 11 \\ 12$$

where  $f_n$  is the normal contact force;  $G$  is the shear modulus;  $\nu$  is the Poisson's ratio and  $r$  is the radius of the grain. A simpler form of stiffness for a spherical grain is defined as:

$$k_n = 4ER \quad (4.3) \quad 15 \\ 16$$

where  $E$  is the Young's modulus of the material and  $R$  is the radius of the grain. The normal damping coefficient  $C_n$  is chosen to give a required coefficient of restitution  $\varepsilon$  (defined as the ratio of the post-collisional to pre-collisional normal component of the relative velocity) for the materials involved:

$$C_n = 2\gamma\sqrt{m_{ij}k_n} \quad (4.4) \quad 21$$

$$\text{where } \gamma = -\frac{\ln(\varepsilon)}{\sqrt{\pi^2 + \ln^2(\varepsilon)}}, \quad \text{and} \quad m_{ij} = \frac{m_i m_j}{m_i + m_j} \quad (4.5) \quad 22 \\ 23$$

10 Discrete Element Method simulations were carried out with columns having different initial aspect ratio 'a', varying from 0.2 to 10. In order to study the effect of crystallisation on the run-out distance, 10 more MD simulations were carried out on granular columns composed of grains arranged on a hexagonal lattice. In order to maintain a threshold amount of grains, in all the cases the columns contain at least 1000 grains, which is the safe lower limit for DEM as suggested by [Oda and Iwashita \(1999\)](#). The micro-mechanical parameters used in this study are presented in Table 4.2. Due to the unsteady nature of the flow, the grains get dispersed on the horizontal plane as discrete bodies start to separate from the main mass, hence the run-out distance is calculated as the position of the farthest grain which has at least one contact with the

Table 4.2 Micromechanical parameters used in Discrete Element Method simulations

Parameter	Value
Young's modulus of glass bead	$70 \times 10^9 \text{ N/m}^2$
Poisson's ratio	0.22 - 0.24
Diameter of glass beads	0.92 to 1.38 mm
Normal and shear stiffness of grains	$1.6 \times 10^8 \text{ N/m}$
Normal and shear stiffness of wall	$4 \times 10^8 \text{ N/m}$
Inter-particle friction coefficient, $\mu$	0.53
Friction coefficient of wall	0.466
Coefficient of restitution, $\Gamma$	0.4

Table 4.3 Parameters used in continuum simulations

Parameters	Value
Number of material points representing an actual particle	4
Material point spacing	0.575 mm
Number of material points per mesh	16
Young's Modulus, E	$1.98 \times 10^6 \text{ Pa}$
Poisson's ratio, $\nu$	0.22 to 0.24
Friction angle, $\phi$	$23.0^\circ$
Dilatancy angle, $\Phi$	$0^\circ$
Density, $\rho$	$1800 \text{ kg/m}^3$
Wall friction	0.466
Time step increment	$1.0 \times 10^{-6}$

<sup>1</sup> main mass. A plane strain collapse of granular column is simulated as a continuum using MPM.  
<sup>2</sup> The effect of number of material points on the accuracy of the simulation was discussed in  
<sup>3</sup> Chapter 4. [Guilkey et al. \(2003\)](#) suggests at least four particles per cell for problems involving  
<sup>4</sup> large deformations. 10 MPM simulations of the granular column collapse were performed using  
<sup>5</sup> Mohr-Coulomb constitutive law by varying the initial aspect ratio, to understand the difference  
<sup>6</sup> between the particle and continuum scale description of granular flows. The parameters used  
<sup>7</sup> for the continuum analyses are presented in Table. 4.3. The Young's modulus of the granular  
<sup>8</sup> assembly is determined by performing a uni-axial compression of the granular column in  
<sup>9</sup> Discrete Element Method.

### <sup>10</sup> 4.2.1 Deposit morphology

<sup>11</sup> The variation of the normalized final run-out distance,  $\Delta L = (L_f - L_i)/L_i$ , with the initial aspect  
<sup>12</sup> ratio 'a' of the column is presented in Figure 4.4. Similar to the experimental results, a power

law relationship is observed between the normalized run-out distance and the initial aspect ratio of the column. However, the molecular dynamics simulations with random packing of grains overestimate the run-out distance by a factor of 1.2. In the present study, the following scaling law for the run-out is observed.

$$\frac{L_f - L_i}{L_i} \approx \begin{cases} 1.67a, & a \lesssim 2.3 \\ 2.5a^{2/3}, & a \gtrsim 2.3 \end{cases} \quad (4.6)$$

The run-out distance observed in the case of hexagonal packing of grains matches the experimental run-out distance observed by [Lajeunesse et al. \(2004\)](#). However, the Discrete Element Method simulations performed with random packing predict longer run-out distances in comparison with the experimental data. The difference in the run-out distance can be attributed to the variation in the packing of grains in the granular column. Although, experimental data corresponds to granular column collapse in a rectangular channel, the collapse is not a pure two-dimensional collapse as in the case of numerical simulations. This can cause some variation in the run-out distance. [Balmforth and Kerswell \(2005\)](#) observed that the material property affects the final run-out distance and included a pre-factor ‘ $\lambda$ ’ in the scaling law, which is in contrast to the observation made by [Lube et al. \(2005\)](#). The scaling law observed in the present study for the random packing is identical to the scaling law observed by [Lajeunesse et al. \(2004\)](#), except for the pre-factor in the scaling law, indicating a strong correlation between the run-out distance and the material property. [Daerr and Douady \(1999\)](#) also observed the effect of initial packing density and the internal structure on the behaviour of granular flows. The continuum description of the granular column collapse using Material Point Method shows good agreement with the experimental results for columns with lower aspect ratio (‘ $a$ ’  $\lesssim 2.3$ ), however it exhibits a significant increase in the run-out distance beyond the aspect ratio of 2.3. [Bandara \(2013\)](#) also observed a jump in the run-out distance at the initial aspect ratio of 2.

In order to understand the mechanism of the run-out in a granular column collapse, it is essential to study the relation between the final collapsed height of the granular column and its initial aspect ratio. Figure 4.5 shows the variation of the normalized final height with the initial aspect ratio of the column. The final height predicted by the Discrete Element Method and the MPM simulations matches the experimental data for granular columns with aspect ratio below 0.7, which indicates that the initial density of the column has negligible effect on the final collapse height. The scaling of final height of the column with the initial aspect ratio of

1 the column can be written as:

$$2 \quad \frac{H_f}{L_i} \propto \begin{cases} a, & a \lesssim 0.7 \\ 3 \quad a^{2/3}, & a \gtrsim 0.7 \end{cases} \quad (4.7)$$

4 The Material Point Method predicts a higher final height of the column in comparison with  
5 the particular simulations that should result in shorter run-outs, however it is inconsistent with  
6 the observations. In case of granular columns with smaller aspect ratios, only a tiny portion of  
7 the total mass is mobilized and the rest remains static, thus predicting the final collapse height  
8 accurately. The final height of a column is controlled by the amount of static region in the  
9 granular column collapse, while the run-out distance is essentially a function of the flowing  
10 mass. Hence, it is essential to compare the evolution of flow and the internal flow structure  
11 in the Discrete Element Method and Material Point Method simulations to understand the  
12 limitations of both the continuum and discrete element approaches.

Figure 4.4 Normalised final runout distance for columns with different initial aspect ratio

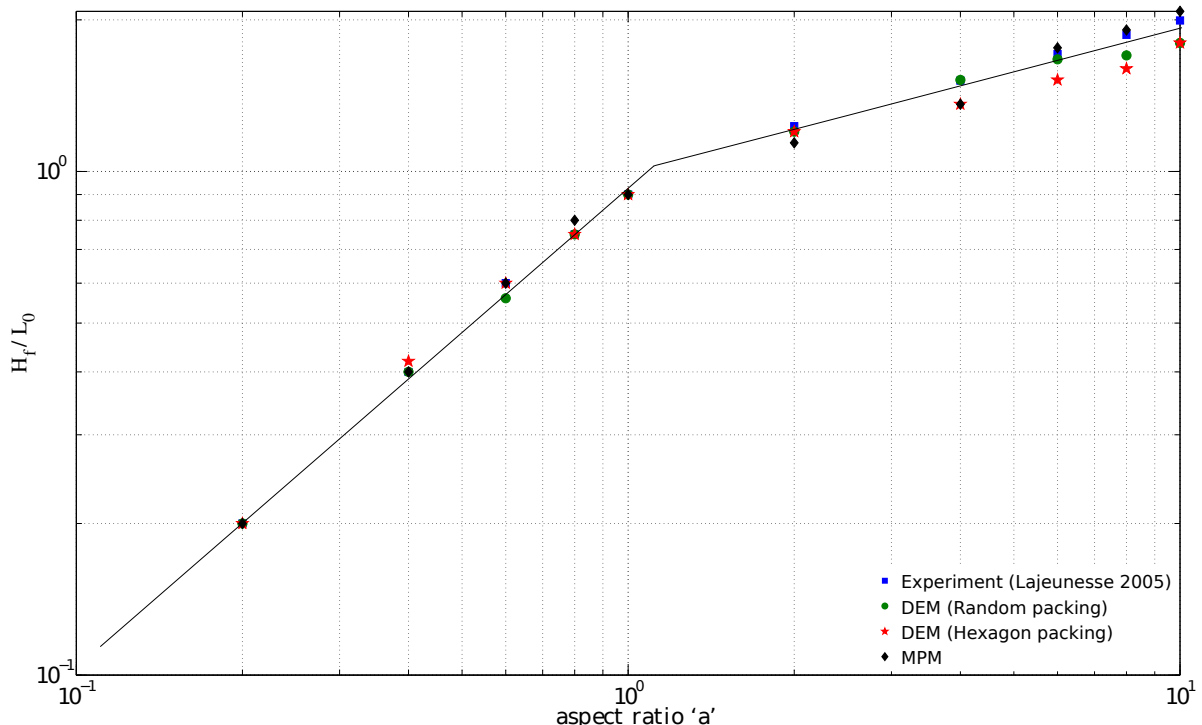


Figure 4.5 Normalised final collapse height for columns with different initial aspect ratio

### 4.2.2 Flow evolution and internal flow structure

For a fixed granular material and substrate properties, the flow dynamics and the final deposit morphology do not depend on the volume of granular material released, but depend only on the aspect ratio ‘ $a$ ’ of the column. A power law relationship is observed between the run-out distance and the initial aspect ratio of the column. A transition in the run-out behaviour at an aspect ratio of 2.3 indicates a change in the flow dynamics. For smaller aspect ratios, the granular mass fails through avalanching of flanks producing a truncated cone-like deposit ( $a' < 0.7$ ) or conical deposit ( $a' > 0.7$ ). At smaller values of aspect ratios, the flow is initiated by failure at the edge of the pile along a well-defined fracture surface. The grains located above the failure surface move “*en masse*” leaving a static region underneath the failure surface. After a transient time of order  $\tau_c$ , defined as  $\sqrt{H_i/g}$ , the flow is fully developed. The velocity profile along the granular column at critical time  $\tau_c$  is presented in Figure 4.6. At critical time, the velocity field depends only on the position of the grain along the sliding mass. The maximum velocity is observed at the front of the flowing mass corresponding to that of a plug flow in horizontal direction. Particulate and continuum simulations yield similar run-out distance at critical time. Unlike particulate simulations, the Material point method predicts that the maximum horizontal velocity occurs at the top of the sliding mass. Behind the fast flowing front, the flow is localized in the mass above the failure surface and the velocity profiles are locally parallel to the failure plane. The flow is composed of upper linear part and a lower exponential tail in the static granular bed. The velocity profile is similar to steady granular surface flow as observed by Lajeunesse et al. (2004).

For columns with lower initial aspect ratios, the run-out distance is proportional to the mass flowing above the failure surface. To understand the amount of mass mobilized during a collapse, the angle of the failure surface has to be studied. Figure 4.6 shows a distinct failure surface when the flow is fully developed at critical time  $\tau_c$ . The angle of the failure surface is found to be about  $55^\circ$ . The failure surface begins from the toe of the column and protrudes inwards at an angle of 50 to  $55^\circ$ . For columns with lower aspect ratios, the formation of the “truncated conical deposit” or “conical deposit” depends only on the initial length of the column, as the angle of the failure surface is found to be independent of the aspect ratio. The failure angle is consistent with the interpretation in terms of *active Coulomb failure* (Lajeunesse et al., 2004), which leads to a predicted failure angle  $\theta_y = 45^\circ + \delta/2$ , where  $\delta$  is the internal friction angle of the granular material. In the present study, the friction angle of the glass beads is  $22^\circ$ , which leads to  $\theta_y = 45^\circ + 22^\circ/2 = 56^\circ$ , which is in good agreement with the numerical simulations and experimental observations by Lajeunesse et al. (2004). Contrary to the suggestion of Lajeunesse et al. (2004), the fracture angle is found to have no direct effect on the transition between the truncated cone and the conical deposit occurring at an aspect ratio

1 of 0.7. [Schaefer \(1990\)](#) observed the onset of instabilities in a narrow wedges of 56 to 65° for  
2 Cambridge type constitutive models that describes granular flows. This observation matches  
3 well with the failure angle observed in the present study. The final profile of the collapsed  
4 granular column with an initial aspect ratio of 0.4 is shown in Figure 4.7. The failure surface is  
5 distinct and the hexagonal dense packing of grains has a steeper failure surface in comparison  
6 with the random packing. The variation observed in the angle of the failure surface causes a  
7 difference in the amount of mobilized mass above the failure surface, and in turn in the run-out  
8 distance. The lower value of run-out distance observed in the case of hexagonal packing of  
9 grains can be attributed to the crystallisation effects. crystallisation is the formation of large-  
10 scale lattice structures during the flow, resulting in non-generic flow patterns. crystallisation is  
11 found to have a significant effect on the final state of the granular column. [Lacaze and Kerswell](#)  
12 ([2009](#)) observed that poly-disperse grains have lesser tendency to crystallize especially in the  
13 case of columns with larger aspect ratio.

14 For larger aspect ratios, the flow is still initiated by a well defined failure surface as can be  
15 seen in Figure 4.8. However, in this case the initial granular column is much higher than the  
16 top of the failure surface. Due to gravity most of the grains in the column fall in the vertical  
17 direction consuming the column along their way. When they reach the vicinity of the failure  
18 surface, the flow gets deviated along the horizontal direction releasing a huge amount of kinetic  
19 energy gained during the free fall. For larger aspect ratio ( $a > 0.7$ ), the resulting static region is  
20 a cone, the final height of the cone, i.e,  $H_f$  lies above the summit of the failure surface. Hence,  
21 a different evolution is observed from that of the axis-symmetric geometry ([Lube et al., 2005](#)),  
22 where the final height coincides with the summit of the failure surface forming a truncated  
23 conical deposit. [Lajeunesse et al. \(2004\)](#) articulated the variation in the deposit morphology  
24 between the axis-symmetric case and the rectangular collapse to be a geometrical effect rather  
25 than as an experimental artefact. The final profile of the collapsed granular column with an  
26 initial aspect ratio of 6 is presented in Figure 4.9. An initial failure surface starting from the toe  
27 end of the column at an angle of about 55° can be observed at critical time  $\tau_c$ . As the collapse of  
28 the granular collapse progresses, successive failure planes parallel to the initial failure surface  
29 are formed and shear failure occurs along these planes. The presence of several shear bands  
30 in the final profile of the collapsed granular column confirms the hypothesis. crystallisation  
31 in hexagonal packing causes a significant effect on the run-out distance by forming series of  
32 parallel shear bands. However, the Material Point Method fails to capture the formation of shear  
33 bands during the collapse. This observation throws light on the mechanics of propagation of  
34 shear bands in massive landslides such as the Storegga submarine landslide. The flow behaviour  
35 becomes similar to that of columns with lower aspect ratio as the flow starts descending along  
36 the failure plane. Regardless of the experimental configuration and the initial aspect ratio of

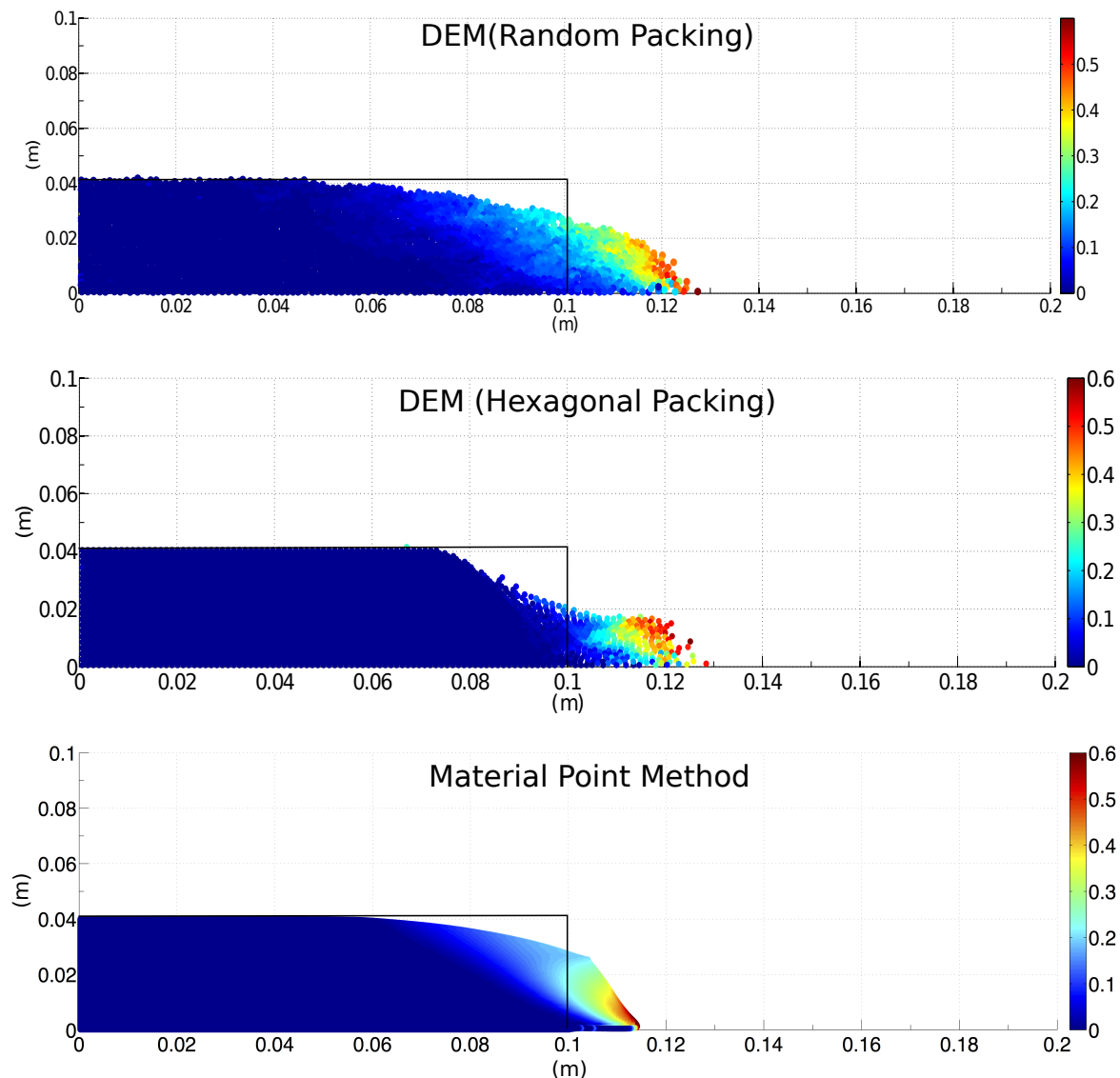


Figure 4.6 Velocity profile of a granular column collapse ( $a' = 0.4 \& t = \tau_c$ )

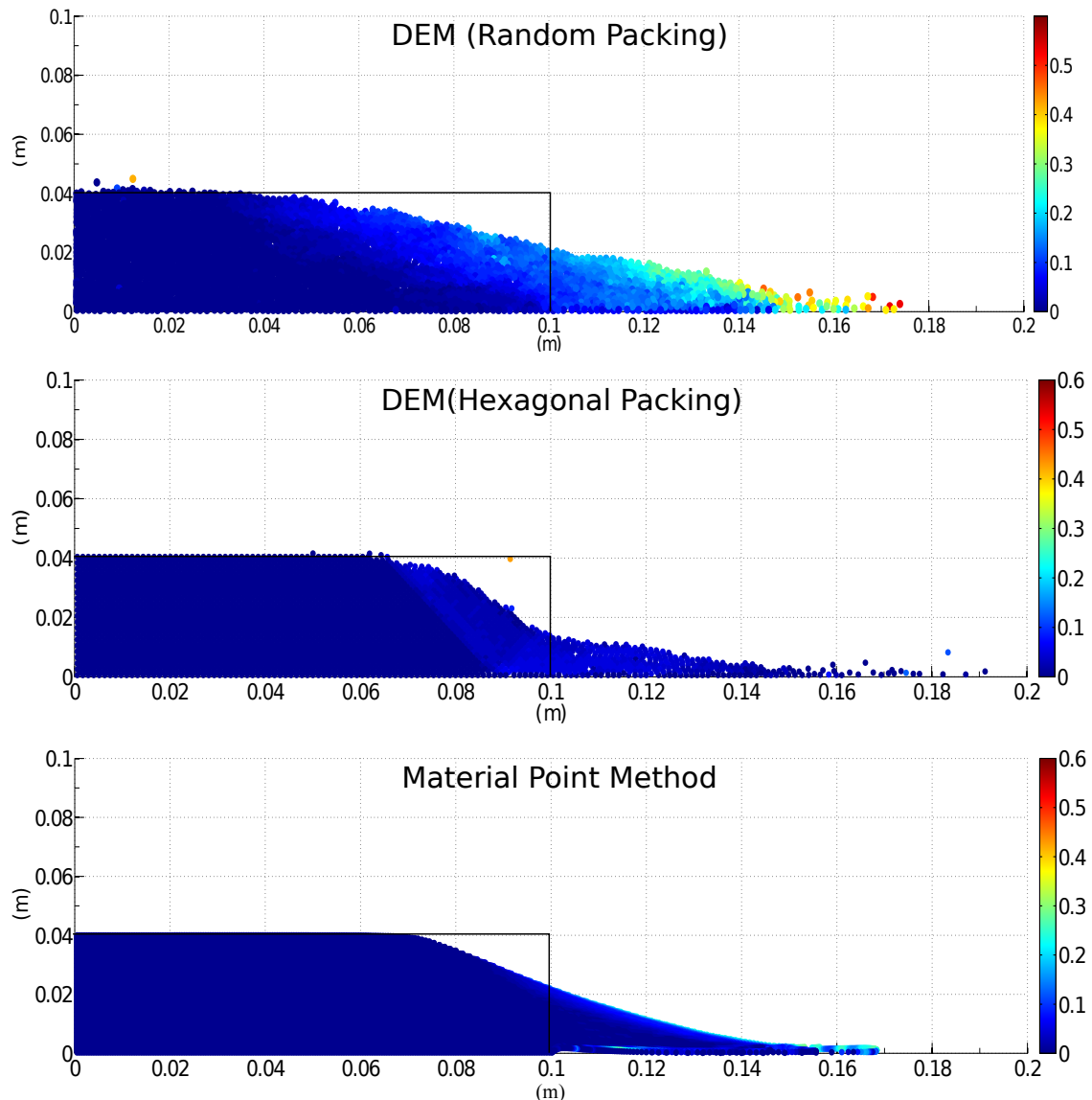


Figure 4.7 Velocity profile of a granular column collapse ( $a' = 0.4$  &  $t = 3 \times \tau_c$ )

the columns, the flow is initiated by a well-defined rupture surface, above which the material slides down leaving a static region underneath the failure plane. Depending on the aspect ratio of the column, two asymptotic behaviours are observed. For smaller aspect ratios, the flow is dominated by friction and by the pressure gradient for larger aspect ratio.

To study the flow dynamics of granular columns with different aspect ratios, the flow front  $L(t)$  and the maximum height of column  $H(t)$  are tracked. The evolution of scaled height ( $H_f/L_i$ ) and the run-out distance  $(L_f - L_i)/L_i$  with time for granular columns with an initial aspect ratio of 0.4 and 6 are presented in Figures 4.10 and 4.11. Time is scaled with respect to the critical time  $\tau_c$ , defined as the time at which the flow is fully mobilized. Three distinct regions can be observed in the flow evolution of granular column collapse regardless of the initial aspect ratio of the column. An initial transient acceleration phase is observed for a time  $0.8\tau_c$ . This phase is followed by a heap movement of granular materials at the foot with a constant spreading velocity  $V$  for about  $2\tau_c$ . When time ' $t$ ' >  $\tau_c$ , the velocity varies linearly with depth in the flowing layer and decreases exponentially with depth near the static layer. This velocity profile is similar to those observed in steady granular surface flows (Lajeunesse et al., 2004). Most of the run-out happens during this phase. The final phase involves deceleration of the flow front and the flow comes to rest after  $0.6\tau_c$ . The spreading of the granular column ceases after a time in the order of  $3\tau_c$  for all values of aspect ratios, however some motion still persists along the free surface behind the flow front for a much longer time due to internal rearrangement, the duration of which can last up to  $t \approx 6\tau_c$ . For smaller aspect ratios, the critical time is evaluated as the point of intersection of the scaled run-out and height. The critical time predicted for both hexagonal and random packing of grains matches the experimental observations. However, the Material Point Method overestimates the critical time by a factor of 1.25, which means that it takes longer for the flow to be fully mobilized. However, the actual run-out duration is short and the granular materials comes to rest abruptly at about  $t = 3\tau_c$ . For columns with larger aspect ratios, the continuum and particulate approaches simulate similar flow evolution behaviour for times up to  $3\tau_c$ , beyond which particulate simulations stabilise and come to rest, while the flow continues to evolve in MPM simulations resulting in larger run-outs than expected. The flow tends to come to rest at time  $t = 6\tau_c$ . The three phases in a granular flow can be distinctly observed in the flow evolution plot for a granular column with initial aspect ratio of 6 (see Figure figure 4.11). For larger aspect ratios, the flow evolution behaviour observed in the case of random packing matches the experimental observation by Lajeunesse et al. (2004). Hexagonal packing predicts longer time for the flow to evolve, which can be attributed to the increase in the internal resistance due to crystallisation of grains. MPM overestimates the critical time by 50%, however has the same value of run-out as the particulate simulations, at time  $t = 3\tau_c$ , beyond which the material continues to flow until it ceases at  $6\tau_c$ . In order to

- <sup>1</sup> understand the flow dynamics in the case of Material Point Method it is important to study the  
<sup>2</sup> effect of different parameters on the deposit morphology.

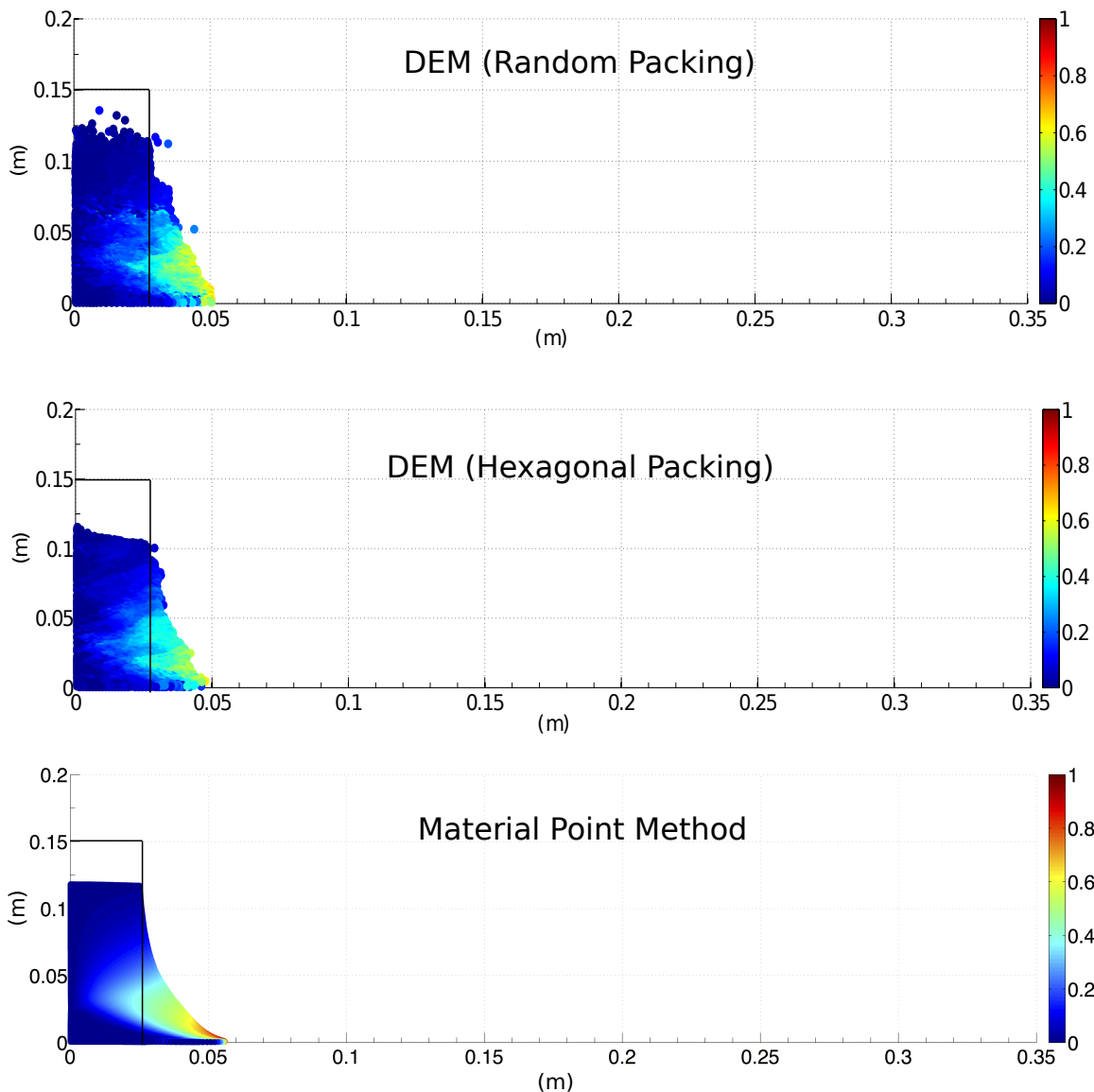


Figure 4.8 Velocity profile of a granular column collapse (' $a' = 6\&t = \tau_c$ )

### <sup>3</sup> 4.2.3 Energy dissipation mechanism

- <sup>4</sup> The time evolution of the flow exhibited three distinct stages during the collapse of a granular  
<sup>5</sup> column. Studying the energy dissipation mechanism provides useful insight into the flow  
<sup>6</sup> dynamics. shows the time evolution of potential energy ( $E_p$ ) and kinetic energy ( $E_k$ ) normalized

## 4.2 Granular column collapse

## 15

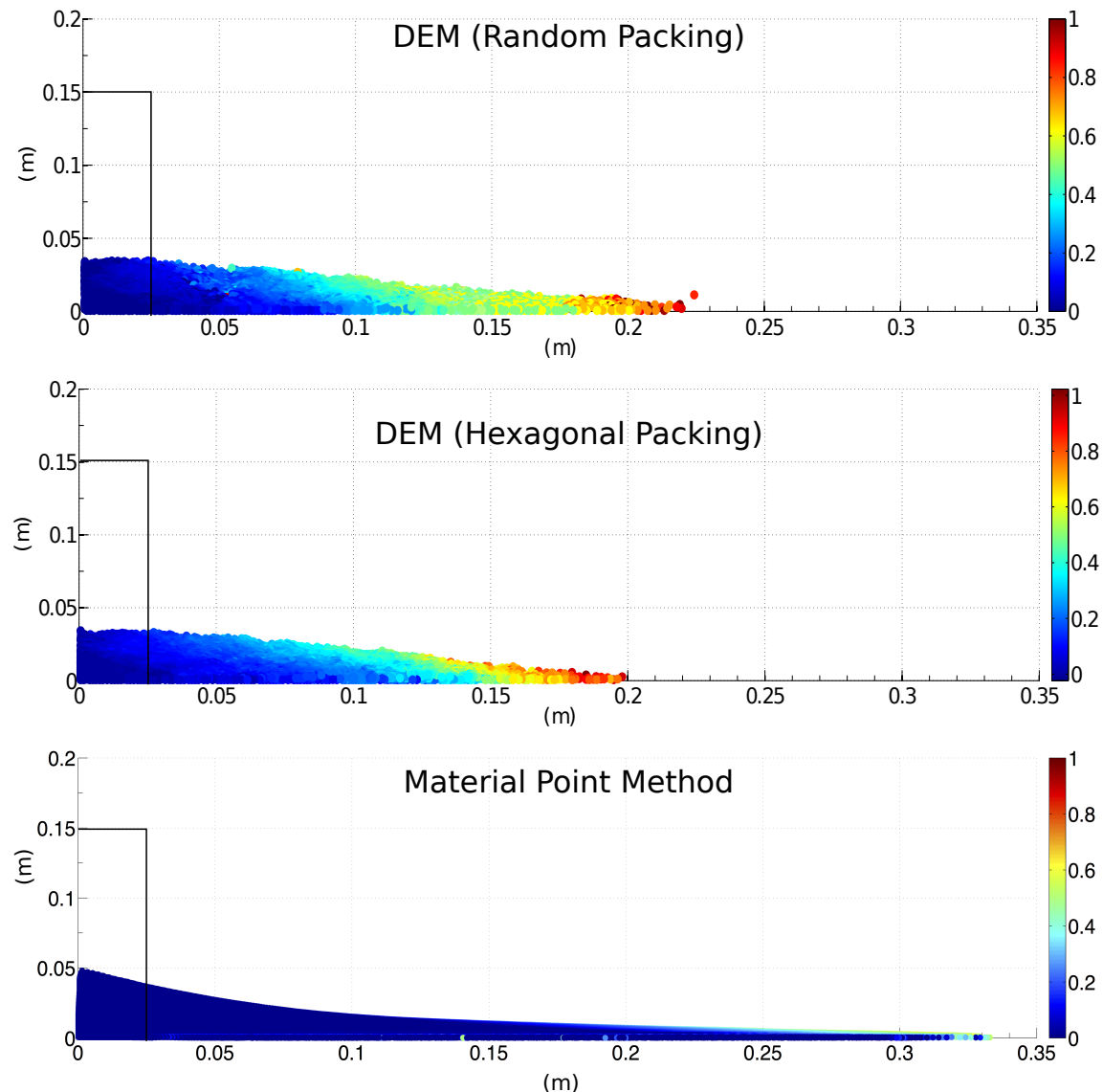
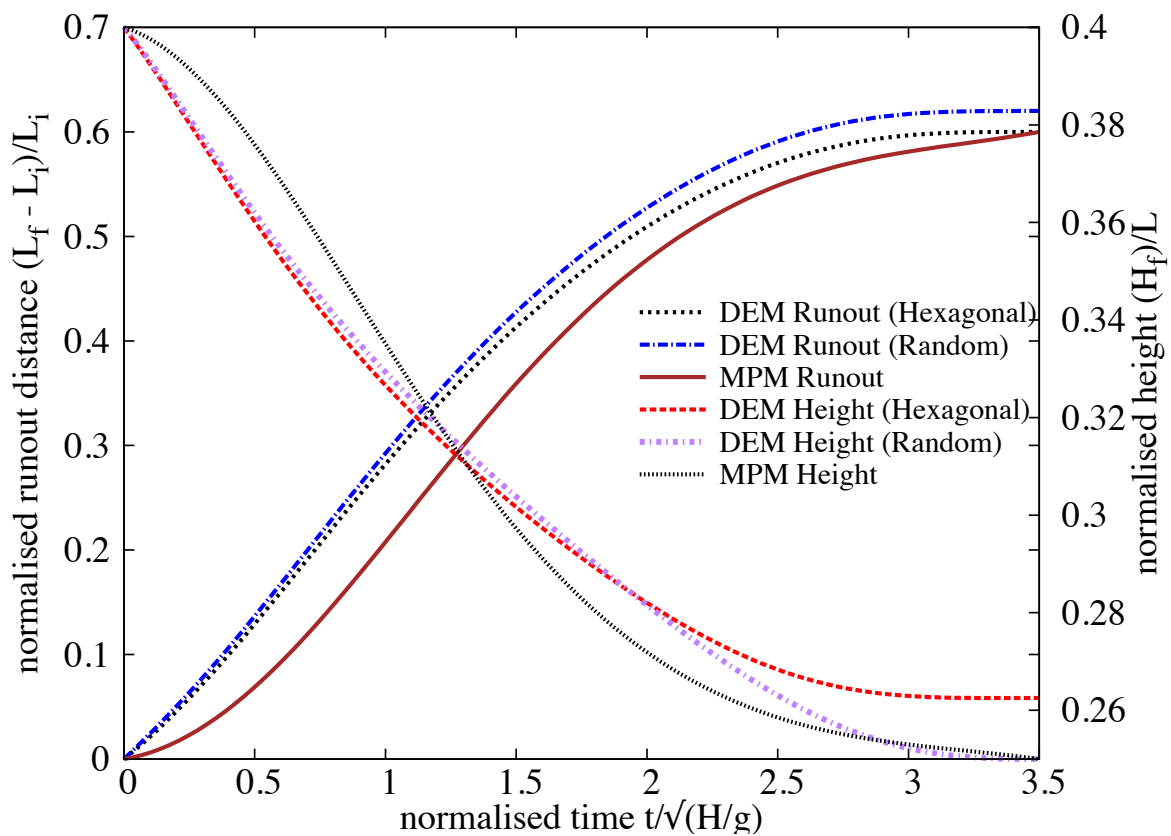
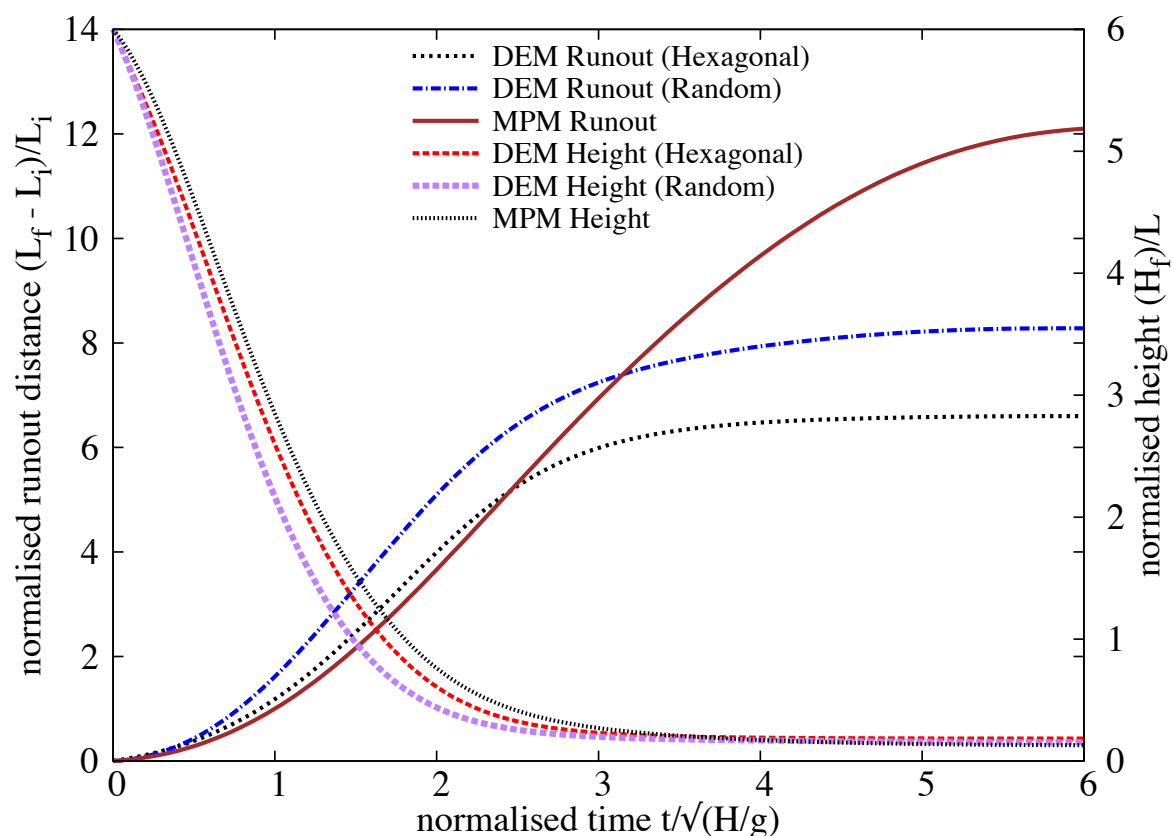


Figure 4.9 Velocity profile of a granular column collapse ( $a' = 6$  &  $t = 3 \times \tau_c$ )

Figure 4.10 Flow evolution of a column with ' $a'$  = 0.4



1 by the initial potential energy  $E_o$ .

$$2 \quad E_p = \sum_{p=1}^{N_p} m_p g h_p \quad (4.8)$$

$$3 \quad E_{ki} = \frac{1}{2} \sum_{p=1}^{N_p} m_p v_p^2 \quad (4.9)$$

4 where  $N_p$  is the total number of particles,  $m_p$  is the mass of a particle ‘ $p$ ’,  $h_p$  is the height and  
 5  $v_p$  is the velocity of the particle ‘ $p$ ’. It can be observed from the figure that the initial potential  
 6 energy stored in the particle is converted to kinetic energy which is dissipated as the granular  
 7 material flows down. Three successive stages can be identified in the granular column collapse.

8 In the initial acceleration stage ( $t < 0.8\tau_c$ ), the initial potential energy stored in the grains is  
 9 converted into vertical motion. In the second stage, the grains undergo collisions with the  
 10 bottom plane and/or with neighbouring grains, and the stored potential energy is converted into  
 11 horizontal motion. In the third stage, the grains eventually leave the base area of the column  
 12 and flow sideways. As the process involves collective dynamics of all the particles, it is difficult  
 13 to predict the exact trajectory of a grain, however, the overall dynamics can be explained. To  
 14 explain the dissipation of energy during the collapse, [Staron et al. \(2005\)](#) assumed that the total  
 15 initial potential energy stored in the system is completely dissipated through friction over the  
 16 entire run-out distance as:

$$18 \quad \mu m_o g \times (L_f - L_i) = m_o g H_o \quad (4.10)$$

19 where  $\mu$  is the friction coefficient. The model predicts well the flow dynamics for columns  
 20 with larger aspect ratios, as most of the initial potential energy is dissipated during the collapse  
 21 involving the entire column. However, for columns with smaller aspect ratios, only a portion of  
 22 the mass above the failure surface is involved in the flow. Hence, the energy dissipation should  
 23 involve only the grains lying above the failure surface. A mathematical model, which considers  
 24 the grains lying above the failure surface, will be derived to predict the flow dynamics of the  
 25 granular column collapse for different aspect ratios.

# References

- Balmforth, N. J. and Kerswell, R. R. (2005). Granular collapse in two dimensions. *Journal of Fluid Mechanics*, 538:399–428. 2  
3
- Bandara, S. (2013). *Material Point Method to simulate Large Deformation Problems in Fluid-saturated Granular Medium*. PhD thesis, University of Cambridge. 4  
5
- Daerr, A. and Douady, S. (1999). Two types of avalanche behaviour in granular media. *Nature*, 399(6733):241–243. 6  
7
- Guilkey, J., Harman, T., Xia, A., Kashiwa, B., and McMurtry, P. (2003). An Eulerian-Lagrangian approach for large deformation fluid structure interaction problems, Part 1: algorithm development. *Advances in Fluid Mechanics*, 36:143–156. 8  
9  
10
- Lacaze, L. and Kerswell, R. R. (2009). Axisymmetric Granular Collapse: A Transient 3D Flow Test of Viscoplasticity. *Physical Review Letters*, 102(10):108305. 11  
12
- Lajeunesse, E., Mangeney-Castelnau, A., and Vilotte, J. P. (2004). Spreading of a granular mass on a horizontal plane. *Physics of Fluids*, 16(7):2371. 13  
14
- Lube, G., Huppert, H. E., Sparks, R. S. J., and Freundt, A. (2005). Collapses of two-dimensional granular columns. *Physical Review E - Statistical, Nonlinear, and Soft Matter Physics*, 72(4):1–10. 15  
16  
17
- Oda, M. and Iwashita, K. (1999). *Mechanics of granular materials: an introduction*. Taylor & Francis. 18  
19
- Schaefer, D. G. (1990). Instability and ill-posedness in the deformation of granular materials. *International Journal for Numerical and Analytical Methods in Geomechanics*, 14(4):253–278. 20  
21  
22
- Staron, L., Radjai, F., and Vilotte, J. P. (2005). Multi-scale analysis of the stress state in a granular slope in transition to failure. *The European physical journal. E, Soft matter*, 18(3):311–20. 23  
24  
25